Computational study on SiH_4 dissociation channels and H abstraction reactions

Toshio Hayashi, Kenji Ishikawa, Makoto Sekine, and Masaru Hori.

Plasma Nano-technology Research Center, Nagoya University, Furo, Chikusa, Nagoya 464-8603, Japan

E-mail: hayashi@plasma.engg.nagoya-u.ac.jp

The primary dissociation channels of SiH_4 were investigated using computational chemistry. The results showed the very similar properties to those of CH_4. The main dissociation product was SiH_2 and the second dissociation product was SiH_3. SiH was produced through SiH_3 to $SiH+H_2$ dissociation by electronic excitation. H abstraction reactions by H and SiH_3 were also calculated for SiH_4, Si_2H_6, Si_3H_8 and Si_9H_{14} (100) cluster model. The energy barriers of H abstraction reactions were lower than those of SiH_3 abstraction reactions. This means considerably important for deposition in SiH_4/H_2 process plasma.

1. Introduction

To understand gaseous reactions in molecules such as CH_4, CF_4, SiH_4, and SiF_4, dissociation channels are substantially important to investigate, therefore many researchers have discussed for a long time. These molecules have T_d symmetrical structure, and are typical examples of symmetrical nonlinear molecules affected by the Jahn-Teller effect. CF_4 and SiF_4 are little affected by the strong Jahn-Teller effect,[1-3] however CH_4 and SiH_4 are strongly affected by the Jahn-Teller effect. Indeed, the vacuum ultraviolet photochemistry of CH_4 and the product channel fields were discussed by Wang et al.[4], in which the quantum yields of distinct product channels were estimated as CH_3+H (0.291), CH_2+H_2 (0.584), CH_2+2H (0.055), and CH+H_2+H (0.07). Exploring potential energy surfaces for photo-dissociation of CH_4 was reported using ab initio studies (multi-configuration self-consistent field method with augmented configuration consistent polarized valence triple-zeta basis set; MCSCF/aug-cc-pVTZ),[5] and multi-configuration time-dependent Hartree (MCTDH) approach.[6] The results support the conclusions of Wang et al. Vacuum ultraviolet spectrum and photochemistry of SiH_4 were reported by many researchers.[7-9] Velasco et al.[7] studies the electronic spectrum of SiH_4 and Jahn-Teller Rydberg series, in which the deformed structures of the C_{2v}, C_s, and C_{3v} symmetry were examined to assign the VUV spectrum, using linear Response Coupled Cluster Single and Double method (CCSDR), molecular-adapted quantum defect orbital (MQDO) approach. Perkins et al.[8] inferred for the 147 nm photolysis of SiH_4 that main dissociation paths were (a) SiH_4 to SiH_2 + 2H (83%) and (b) SiH_4 to SiH_3 +H (13%), whereas the dissociation path of SiH_4 to SiH_2 + H_2 was completely ruled out, because the quantum yields for the decomposition of SiH_4 was estimated at approximately 4 ($4SiH_4$ molecules decomposition per one photon). In view of plasma process, Doughty and Gallagher[9] considered causes of SiH_4 dissociation in silane dc discharges, using mass spectrometry, and emission intensity profiles of SiH^* and H^* (653 nm) were very similar, so that the dissociation of SiH_4 to SiH^* + H_2 + H^* was inferred in the dc discharge plasma. However, they concluded that principal dissociation pathway appeared to be SiH_2 + 2H, based on the results of Perkins et al.[8] Doyle et al.[10] also concluded the inferred dissociation fragmentation was 0.83 to SiH_2 +2H and 0.17 to SiH_3 + H, based on a kinetic modeling of their system and on the 147-nm (8.4-eV) photo-dissociation experiments of Perkins et al.[8] Tsuda, et al,[11] studied the primary process in the plasma-chemical and photochemical vapor deposition from silane, using RHF/3-21G+(*) and 6-21G+(*) to estimate the production root of radiative species Si* ($^1P^o$). Though these reports have been

presented, the primary dissociation channels of SiH_4 in the process plasma are still ambiguous.

The most abundant radical is SiH_3 in the SiH_4 containing plasma, in view of published data obtained by many measurement methods; mass spectrometric measurements,[12-15] optical emission spectroscopy,[13,16-18] laser induced florescence spectroscopy10,[19-21] infrared diode laser absorption spectroscopy,[22-24] cavity ring down spectroscopy.[25,26] However, as aforementioned, it was pointed out that the main dissociation product was SiH_2+2H, based on the results of Xe photolysis of SiH_4 by Perkins et al.[8] Therefore, the main dissociation product channels of SiH_2 and SiH_3 have still been controversy.

H abstraction reaction is also controversy for a-Si and μc-Si deposition process. In general, SiH_3 is also thought to be the main reactant to abstract H atom from the hydrogenated Si surface, because of the most abundant radicals and the low reactivity with the other SiHx molecules in the plasma.[9, 24]

2. Calculation methods

We used electron of motion coupled cluster single and double method (EOMCCSD) with augmented correlation consistent polarized valence double or triple zeta basis set (aug-cc-pVXZ (X=D or T)) to clarify the observed VUV spectrum, employing the deformed structures with C_{2v}, C_{3v}, and C_s symmetry, and the potential surfaces along the deformed structures were calculated to clarify the primary dissociation channels of SiH_4. We also calculated reaction potentials of H and SiH_3 with SiH_4, Si_2H_6, Si_3H_8 and Si_9H_{14} (100) cluster model, using density functional method (DFT) to clarify the H abstraction reaction, using Gaussian09 program.[27]

3. Results and discussion

3.1 Primary dissociation channels of SiH_4

Figure 1 shows the observed vacuum ultra-violet (VUV) spectrum of SiH_4 reported by Cooper et al.[28] it can be seen from this figure that the assignment of the electron transition is very difficult and the excited states are affected by the strong Jahn-Teller effect. The assignment for the VUV spectrum has been examined by many researchers.[7, 29-33] Velasco et al.[7] performed to provide data necessary for a better understanding of the electronic spectrum of SiH_4, by selecting an adequate distorted C_{2v} geometry and using ab initio and density functional methods. The three lower Koopmans ionization potentials were evaluated and vertical excitation energies for the different Rydberg series converging to the

three Jahn-Teller components were inferred. However, the dissociation channels were not fully discussed.

Therefore, we calculated to clarify the dissociation channels of SiH_4 using the EOMCCSD/aug-cc-pVXZ (X=D or T). First, supposing the deformed structures to represent the observed VUV spectrum, we employed the deformed structures with the symmetry of C_{3v}, C_{2v}, and C_s shown in Fig.2. Figure 3 shows the calculated VUV spectrum composed of a C_{2v} deformed structure along wagging mode (a) (60%), a C_{2v} one along stretching mode (b) (10%), a C_{3v} one along Si-H stretching mode (c) (25%), and a C_s one along H-Si-H wagging mode (d) (5%). Assuming the transition probability to triplet excited states on the lower spectrum side depicted by the dashed line, the observed VUV spectrum seems to be almost represented.

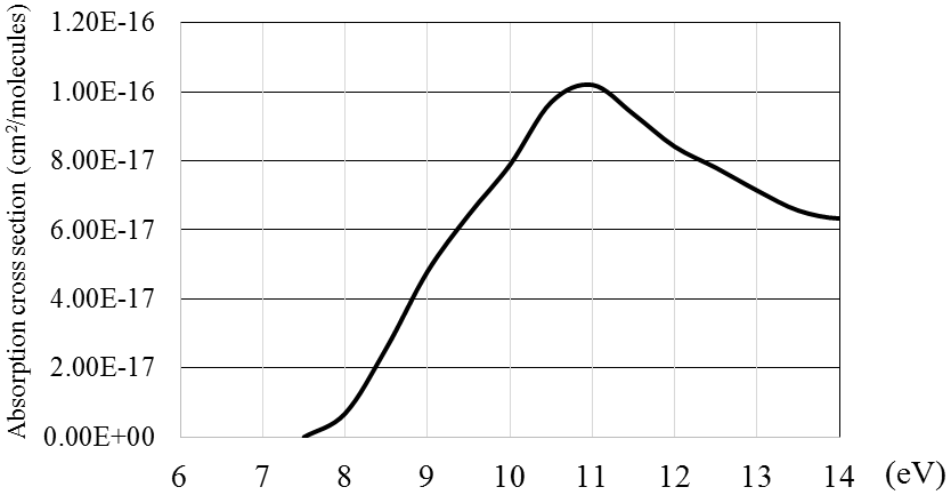

Fig. 1. Observed VUV spetrum[28)]

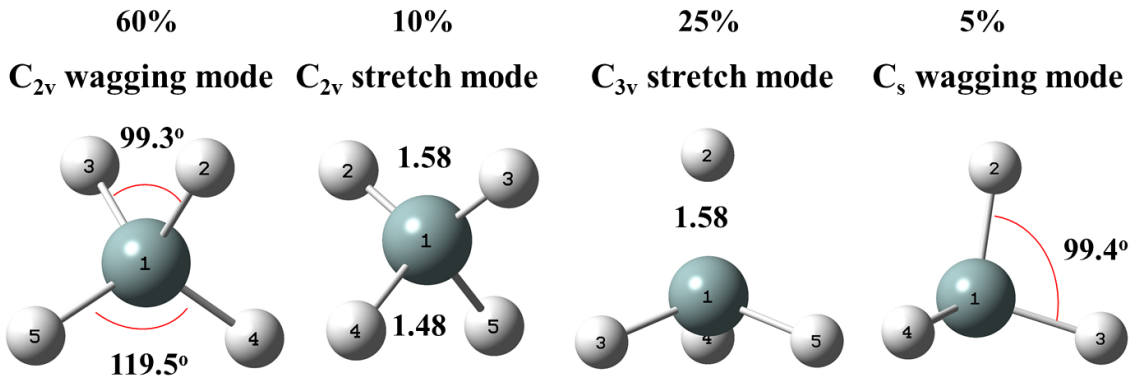

Fig. 2 Employed deformed structures to calculate VUV spectrum.

It can be seen from the Fig. 3 that the deformed structure along C_{2v} wagging mode is very

important to represent the observed VUV spectrum. If the contribution of this transition is lower than 60%, then the monotonously increasing spectrum from the onset to 11 eV cannot be represented. Therefore, the excitation probability at this deformed structure affected by strong Jahn-Teller effect may be 60% or more. This result may consistent with the prediction by Velasco et al.[7)]

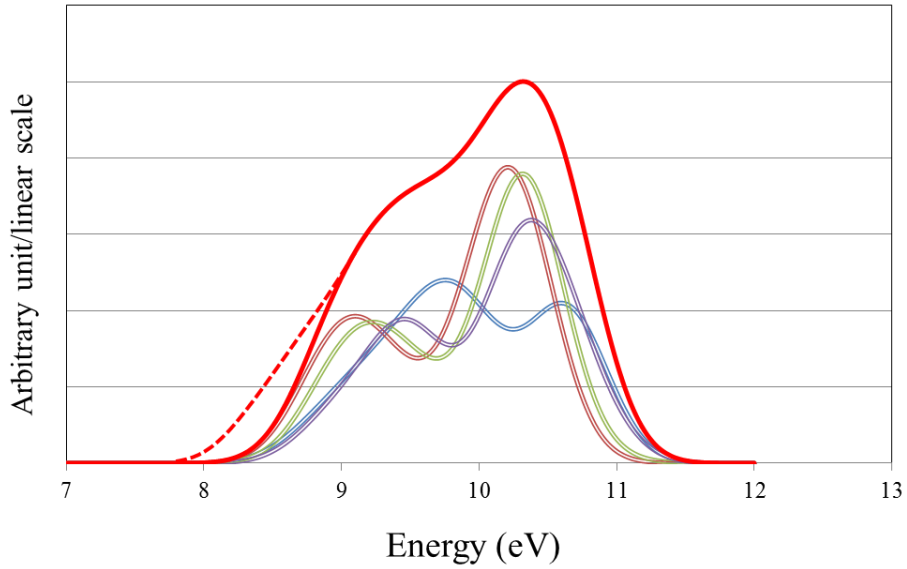

C_{2v}(wagging) 60% + C_{2v}(stretching) 10% + C_{3v}(stretching) 25% + C_s (stretching) 5%, C_{2v} (wagging), C_{2v} (stretching), C_{3v} (stretching), C_s (stretching)

Fig. 3 Calculated VUV spectrum of SiH_4, using the deformed structures shown in Fig.2. The dashed line shows the supposed transition probability to the triplet excited states. The higher energy levels than 10.5 eV were not calculated here. The solid line shows the sum of the calculated VUV spectral intensities along the deformed structures depicted in Fig. 2.

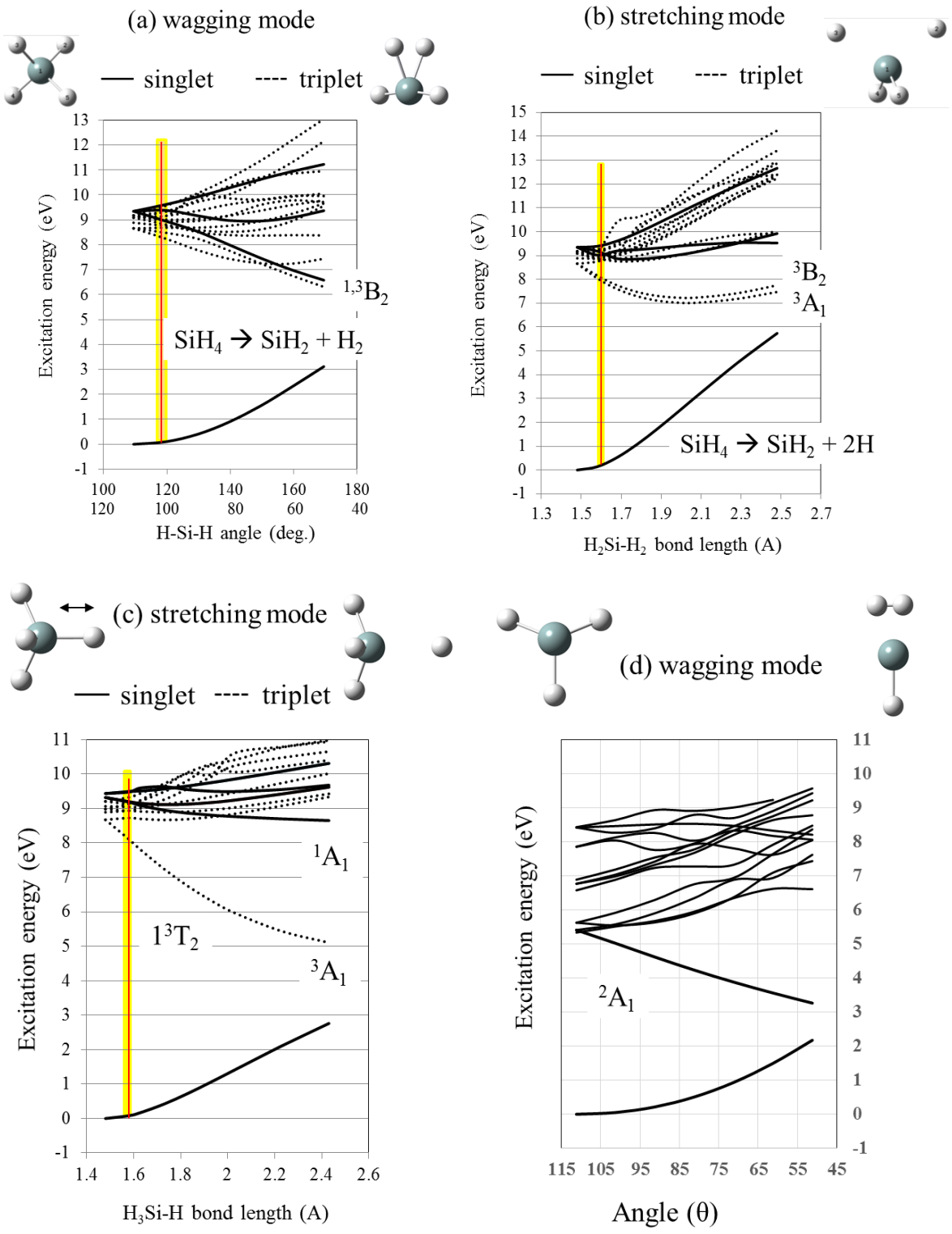

Fig. 4 The calculated potential surfaces for the excited states along (a) C_{2v} wagging mode, (b) C_{2v} stretching mode, (c) C_{3v} stretching mode of SiH_4, and (d) D_{3h} to C_{2v} wagging mode of SiH_3 radical.

Figure 4 shows the potential curves for the excited states along the C_{2v} wagging mode (a), C_{2v} stretching mode (b), C_{3v} stretching mode (c) of SiH_4, and C_{2v} wagging mode of

SiH_3 radical (d) calculated using EOMCCSD/aug-cc-pVDZ as a function of H-Si-H angle and Si-H bond length, respectively. The transition energies to low lying excited state were also calculated by EOMCCSD/aug-cc-pVTZ, and it was confirmed the same transition energies were obtained. The higher transition energies than 11 eV were not shown here, because the higher transition states than 11 eV are not precisely represented without higher Rydberg orbitals and also the dissociative properties in the low lying excited states is very important in view of electron energy distribution function of the process plasma. The vertical lines in these figures are the excitation points with the deformed structures depicted in Fig. 2. Comparing these figures, the lowest singlet and triplet excited states along the C_{2v} wagging mode are monotonously dissociative, so SiH_4 preferentially dissociates as excitation to these states takes place by electron collisions in the process plasma. In the case of the excitation along the C_{3v} stretching mode, the lowest triplet state is preferably dissociative, so the excitation to this state takes place that SiH_4 dissociates to SiH_3 + H. This result is consistent with that obtained Xe photolysis of SiH_4 reported by Perkins et al.[8)] and Nomura et al.[23)] Excitation probability to singlet states is larger than those to triplet states and the dissociative tendency is depend on the gradient of the excited state potential surface. Therefore, the potential surfaces for the excited states along these deformed structures show the very similar dissociation properties to those of CH_4; the product channels are supposed as the order of SiH_2+H_2 > SiH_3+H > SiH_2+2H. This result is inconsistent with the inferences of Doughty and Gallagher [9)] and Doyle et al.[10)] However, it can be seen from Fig. (4) (b) that the dissociation path of SiH_2 +2H is hard to take place via the lowest singlet state. Therefore, our results for the dissociation tendency seem to be more realistic. Furthermore, this product channels are not proportional to the observed radical densities in the SiH_4 plasma,[9,24)] in which SiH_3 is the most abundant radical and the density of SiH_2 is very low. This is due to the high reaction probability of SiH_2 + SiH_4 to Si_2H_6,[34)] as pointed out by earlier research results. SiH radical may be produced by one or two step reaction, produced via the lowest excited states of SiH_3 along H-Si-H waging vibrational mode, as denoted in Fig. 4 (c) and (d). Under the low pressure condition in which three body reaction does not take place, excited SiH_3 (D_{3h}) radical is produced on the dissociation pathway and then dissociates to SiH + H_2 reaction in one step reaction. If the energy quenching takes place through three body reaction under the high pressure condition, two step reactions may take place.

3.2 Reactions in the gas phase and on the surface

Figure 5 shows reaction potentials of SiH_4 + SiH_2 (a) and Si_2H_6 + SiH_2 (b) calculated

using B3LYP/6-311+G(d,p). These reaction potentials are consistent with the suggestion from the measured radical density in which the density of SiH_2 is lower than that of SiH_3.[24)]

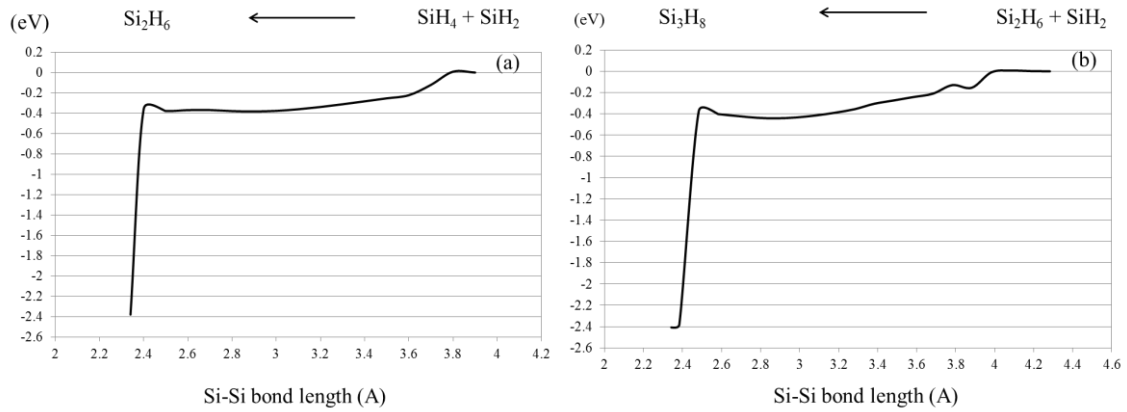

Fig. 5 Reaction potentials of $SiH_4 + SiH_2$ to Si_2H_6 (a) and $Si_2H_6 + SiH_2$ to Si_3H_8 (b).

On the other hand, H abstraction reaction in the gas phase and on the surface is a little controversy. In general, it is believed that H abstraction reaction is mainly caused by SiH_3 radical, not H atom. Figure 6 is the reaction potential of $SiH_4 + H$ (a), $Si_2H_6 + H$ (b), and $Si_3H_8 + H$ (c). In the case of $SiH_4 + H$ reaction, the activation energy of the reaction is calculated as 0.11 eV by B3LYP/6-311+G(d,p), which gives generally lower energy than the experimental value.[35)] Arrhenius parameters for the reaction of H atoms and SiH_4 were reported by Arthur and Miles,[36)] in which the Arrhenius rate expression was presented with the activation energy of 0.16 eV. However, the activation energies of $Si_2H_6 + H$ and $Si_3H_8 + H$ are almost nothing in our DFT calculations.

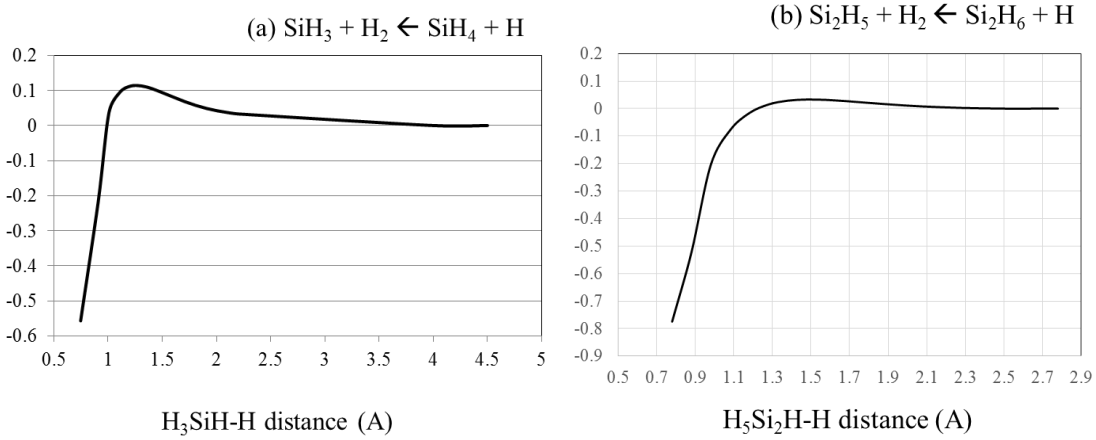

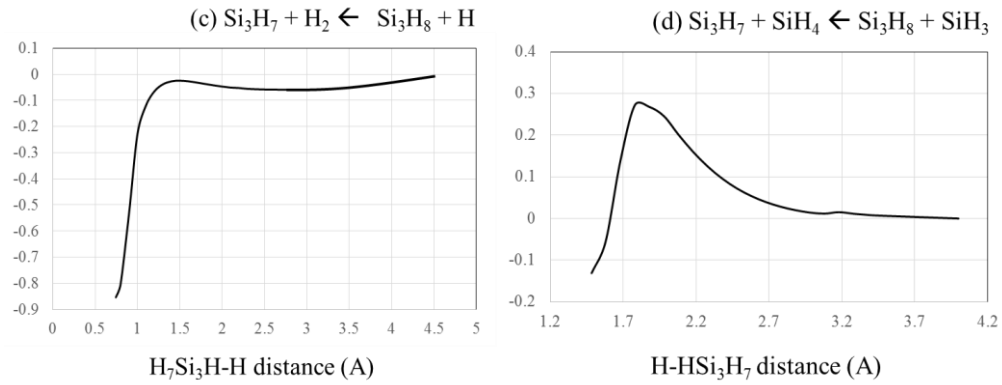

Figure 6 Calculated reaction potentials for SiH_4 + H to SiH_3 + H_2 (a), Si_2H_6 + H to Si_2H_5 + H_2 (b), Si_3H_8 + H to Si_3H_7 + H_2 (c), and Si_3H_8 + SiH_3 to Si_3H_7 + SiH_4 (d), using B3LYP/6-311+G(d,p).

On the other hand, the activation energy of Si_3H_8 + SiH_3 reaction is calculated as 0.272 eV by B3LYP/6-311+G(d,p), shown in Fig. 6 (d). The calculated basis set super position error (BSSE) is 0.014 eV (B3LYP/6-311+G(d,p)) and 0.06 eV (EOMCCSD/aug-cc-pVDZ) at the transient point. Therefore, the activation energy for this reaction may be approximately 0.33-0.35 eV at the transient point. In the process plasma, thermally activated H atoms over 0.2eV may be produced by electron excitation dissociations of SiH_4 and H_2, and H_2 and SiH_4 are also thermally activated around the heated substrate. Therefore, the H abstraction reaction from SiH_4, Si_2H_6 by H atoms in the gas phase could not be ignored.

Figure 7 shows the potential curves of H abstraction reactions calculated using B3LYP/6-311+G(d,p) and Si_9H_{14} (100) cluster model. The H abstraction reaction by H atom does not show the potential barrier (Fig. 8 (a)), however, the H abstraction by SiH_3 radical shows the small potential barrier of 0.1 eV. As mentioned above, the activation energy calculated using B3LYP method and without BSSE correction is generally lower than the experimental value. Bakos et al. reported the activation energy of approximately 0.4 eV using Si_9H_{14} (100) cluster model and density functional method.[37)]

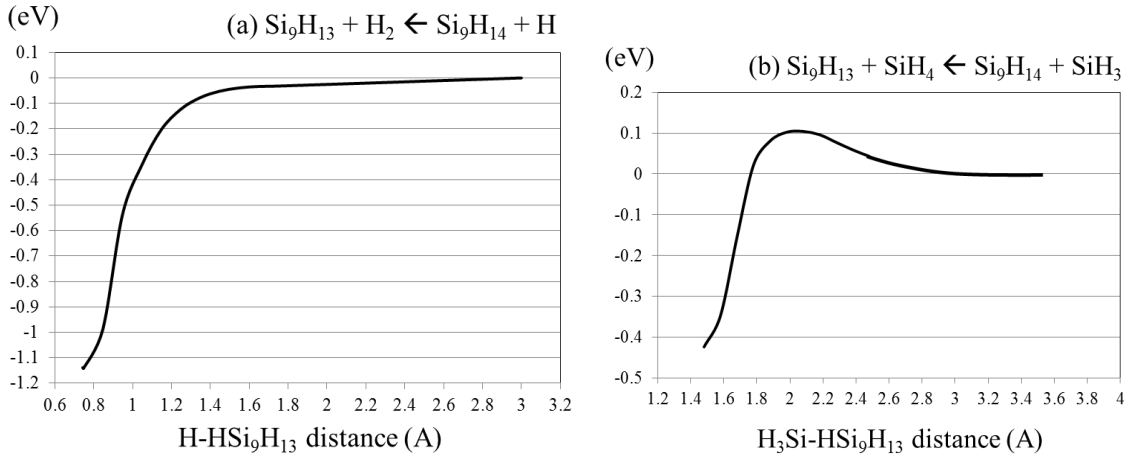

Fig. 7 Reaction potentials for Si_9H_{14} (100) + H to Si_9H_{13} + H_2 and Si_9H_{14}(100) + SiH_3 to Si_9H_{13} + SiH_4, calculated using B3LYP/6-311+G(d,p).

This means the abstraction reaction of H atoms on a-Si is hardly caused by SiH_3 radical, and preferably caused by H atoms on the low temperature substrate in SiH_4/H_2 process plasma, and also means SiH_3 radical is less reactive and therefore has the long life time. The potential barrier of insertion reaction of H atom to -Si-Si- bond is also very low. For example, the activation energy of Si_3H_8 + H to Si_2H_5 + SiH_4 reaction is approximately 0.15 eV, reported by Varma et al.[38] These results mean that H atom is very reactive to cause H abstract reaction and insertion reaction to -Si-Si- bond in the SiH_4/H_2 process plasma. On the other hand, SiH_3 is less reactive, compared with H atom for the H abstract reaction. However, H abstract reaction by SiH_3 may take place on the heated substrate and under the H depleted process condition, because of the relatively low activation energy. Under the appropriately balanced condition of H abstract reaction and H insertion reaction, SiH_3 acts as the film precursor leading to μ-crystalline film growth.[39]

Figure 8 shows the potential surfaces for negative and positive ions of SiH_4 as a function of Si-H bond distance, along SiH_4^+ (C_{3v}) to SiH_3^+(D_{3h}) + H and SiH_4^+ (C_s) to SiH_2^+(C_{2v}) + H_2 deformation. The potential surfaces of the ground state, negative ion state, and vertical positive ion state were calculated as a function of Si-H bond distance along the SiH_4 (T_d) to SiH_3 (C_{3v}) + H deformation, using EOMCCSD/aug-cc-pVDZ. The observed appearance energy of SiH_2^+ and SiH_3^+ is 11.5-11.6 eV and 11.9-12.0 eV, respectively.[40,41] Therefore, SiH_2^+ ion is preferably produced in the threshold energy region. However, ionization cross sections of both ions are almost the same in the higher energy region.[15] The structure of SiH_4^+ ion at the vertical ionization region was hard to optimize. This may be due to the Jahn-Teller effect for the ionized state.[42, 43] The vertical dashed line in Fig. 8 denotes the

assumed ionization position deformed along SiH_4^+ (C_{3v}) to SiH_3^+(D_{3h}) + H (shown by the molecular structures at upper site) and SiH_4^+ (C_s) to SiH_2^+(C_{2v}) + H_2 (shown by the molecular structures at lower site). The negative ion does not show dissociative properties at the low lying vertical electron attachment region. If the fragmented negative ions are observed, the higher excited (Rydberg) states may contribute as ion pair formations.[44)]

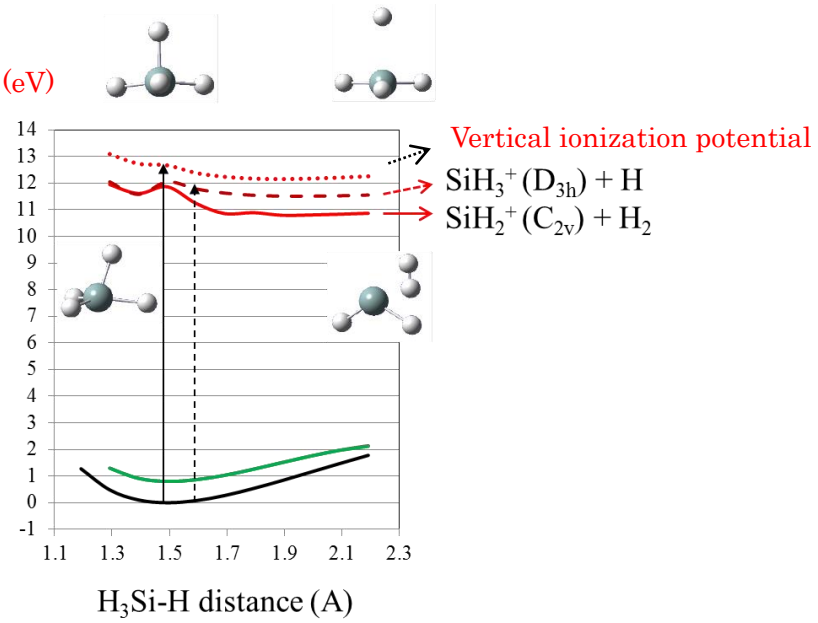

Fig. 8 Potential surfaces for negative and positive ions of SiH_4 as a function of Si-H bond distance, along SiH_4^+ (C_{3v}) to SiH_3^+(D_{3h}) + H and SiH_4^+ (C_s) to SiH_2^+(C_{2v}) + H_2 deformation, obtained using EOMCCSD/aug-cc-pVDZ.

4. Conclusions

The primary dissociation channels of SiH_4 were investigated using computational chemistry (EOMCCSD/aug-cc-pVDZ and B3LYP/6-311+G(d,p). SiH_4 molecule is a typical example of symmetrical nonlinear molecules affected by the Jahn-Teller effect. Therefore, the deformed structures were estimated to represent the observed VUV spectrum, and then the potential surfaces for the excited states were calculated along the deformed structures to clarify the product channels. The results showed the very similar properties to those of CH_4. The main dissociation product was SiH_2 and the second dissociation product was SiH_3. SiH was produced through SiH_3 to SiH+H_2 dissociation by electronic excitation.

This result is inconsistent with the observed radical density. Therefore, reaction potentials of SiH_2 with SiH_4 and Si_2H_6 were calculated using density functional method (B3LYP/6-311+G(d,p)), and it was clarified that the exothermic reactions took place

without activation energy; the high reaction probability of SiH_2 with SiH_4 and Si_2H_6 and the low reaction probability of SiH_3 radical were confirmed. This is the reason for the inconsistency.

H abstraction reactions in the gas phase and on the surface were also examined using DFT method. The results showed the abstraction reaction of H atoms in the gas phase and on the surface is hardly caused by SiH_3 radical, and preferably caused by H atom on the low temperature substrate in SiH_4/H_2 process plasma, and also showed SiH_3 radical is less reactive and therefore has the long life time. Therefore, it is concluded that the H abstraction reaction by H atom cannot be ignored.

Ionization process of SiH_4 is also a matter of argument. The calculated results obtained using EOMCCSD/aug-cc-pVDZ showed that SiH_2^+ ion was preferably produced rather than SiH_3^+ ion in the threshold energy region. This is caused by Jahn-Teller effect of SiH_4^+ ion.

Acknowledgment

The authors express a great appreciation to Prof. Hitoshi Itoh of Nagoya University for his advice on the reactions on Si surface.

References

1) N. Watanabe, D. Suzuki, and M. Takahashi, J. Chem. Phys. 134, 064307 (2011).
2) T. Hayashi, K. Ishikawa, M. Sekine, and M. Hori, *proceedings of 35th International Symposium on Dry process* (2013, Jeju) p-64.
3) K. Kameta, M. Ukai, T. Numazawa, N. Terezawa, Y. Chikahiro, N. Kouchi, and Y. Hatano, J. Chem. Phys. 99, 2487 (1993).
4) J. H. Wang, K. L., Z. Min, H. Su, R. Bersohn, J. Preses, and J. Z. Larese, J. Chem. Phys. **113**, 4146 (2000).
5) A. M. Velasco, J. Pitarch-Ruiz, A. M. J. Sánchez de Merás, J. Sánchez-Marín, and I. Martin. J. Chem. Phys. **124**, 124313 (2006).
6) R. van Harrevelt, J. Chem. Phys. **125**, 124302 (2006).
7) A. M. Velasco, C. Lavín, A. M. J. Sánchez de Merás, and J. Sánchez Marín. J. Chem. Phys. **135**, 214304 (2011).
8) G. G. A. Perkins, E. R. Austin, and F. W. Lampe, J. Am. Chem. Soc. 101, 1109 (1979).
9) D. A. Doughty and A. Gallagher, Phys. Rev. A **42**, 6166 (1990).
10) J. R. Doyle, D. A. Doughty, and A. Gallagher, J. Appl. Phys. **68**, 4375 (1990)
11) M. Tsuda, S. Oikawa, and K. Sato, J. Chem. Phys. **91**, 6822 (1989).
12) B. Drevillon, J. Huc, A. Lloret, J. Perrin, G. de Rosny, and J. P. M. Schmitt, Appl. Phys. Lett. **37**, 646 (1980)
13) A. Matsuda and K. Tanaka, Thin Solid Films. **92**, 171 (1982).
14) H. Chatham, D. Hils, R. Robertson, and A. Gallagher, J. Chem. Phys. **81**, 1770 (1984).
15) E. Krishnakumar and S. K. Srivastava, Contrib. Plasma. Phys. **35**, 395 (1995).
16) J. Perrin and J.P.M. Schmitt, Chem. Phys. **67**, 167 (1982).
17) T. Sato and T. Goto, Jpn. J. Appl. Phys. **25**, 937 (1986).
18) W. M. M. Kessels, M. C. M. van de Sanden, and D. C. Schram, J. Vac. Sci. Technol. A **18**, 2153 (2000).
19) Y. Matsumi, T. Hayashi, H. Yoshikawa, and S. Komiya, J. Vac. Sci. Technol. A **4**, 1786 (1986).
20) K. Tachibana, T. Mukai, and H. Harima, Jpn. J. Appl. Phys. **30**, L1208 (1991).
21) A. Kono, N. Koike, K. Okuda, and T. Goto, Jpn. J. Appl. Phys. **32**, L543 (1993).
22) N. Itabashi, N. Nishiwaki, M. Magane, T. Goto, A. Matsuda, C. Yamada, and E. Hirota, Jpn. J. Appl. Phys. **29**, 585 (1990).
23) H. Nomura, A. Kono, and T. Goto, Jpn. J. Appl. Phys. **33**, 4165 (1994).
24) M. Hori1 and T. Goto, Plasma. Source. Sci. Technol. **15**, 574 (2006).
25) W. M. M. Kessels, A. Leroux, M. G. H. Boogaarts, J. P. M. Hoefnagels, M. C. M. van de Sanden, and D. C. Schram, J. Vac. Sci. Technol. A **19**, 467 (2001).
26) W. M. M. Kessels, J. P. M. Hoefnagels, M. G. H. Boogaarts, D. C. Schram, and M. C. M. van de

Sandenb, J. Appl. Phys. **89**, 2065 (2001).

27) Gaussian09,Rev. A.1, Gaussian, Inc., Wallingford CT, (2009).

28) G. Cooper, G. R. Burton, W. F. Chan, and C. E. Brion., Chem. Phys. **196**, 293 (1995).

29) M. Suto and L. C. Lee, J. Chem. Phys. **84**, 1160 (1986).

30) U. Itoh, Y. Toyoshima, H. Onuki, N. Washida, and T. Ibuki, J. Chem. Phys. **85**, 4867 (1986).

31) C. Larrieu, D. Liotard, M. Chaillet, and A. Dargelos, J. Chem. Phys. **88**, 3848 (1988).

32) H. Ishikawa, K. Fujima, H. Adachi, E. Miyauchi, and T. Fujii, J. Chem. Phys. **94**, 6740 (1991).

33) L. Chantranupong, G. Hirsch, R. J. Buenker, and M. A. Dillon, Chem Phys. **170**, 167 (1993).

34) K. Matsumoto, S. J. Klippenstein, K. Tonokura, and M. Koshi, J. Phys. Chem. A **109**, 4911 (2005).

35) F. Janssen, *Introduction to Computational Chemistry* (Wiley, England, 2007) 2nd ed., p258.

36) N. L. Arthers and L. A. Miles, J. Chem. Soc. Farady Trans. **93**, 4259 (1997).

37) T. Bakos, M. S. Valipa, and D. Maroudas, J. Chem. Phys. **122**, 054703 (2005).

38) D. H. Varma, P. Raghunath, M. C. Lin, J, Phys. Chem. A **114**, 3648 (2010).

39) A. Matsuda, Jpn. J. Appl. Phys. **43**, 7909 (2004).

40) J. Berkowitz, J. P. Greene, H. Cho, and B.Ruscic, J. Chem. Phys. **86**, 1235 (1987).

41) S. K. Shin, R.R. Corderman, and J. L. Beauchamp, Int. J. Mass Spectrom. Ion Processes, **101**, 257 (1990).

42) . R. Caballol, J. A. Catala and J. M. Problet, Chem. Phys. Lett. **130**, 278 (1986).

43) F. De Proft, and P. Geerlings, Chem. Phys. Lett. **262**, 782 (1996).

44) M. Hoshino, S. Matejcik, Y. Nunes, F, Ferreira da Silva, P. Limao-Vieira, and H. Tanaka, Intern. J. Mass Spectrom.**306** 51 (2011).

Figure Captions

Fig. 1. Observed VUV spetrum[28)]

Fig. 2. (Color online) Employed deformed structures to calculate VUV spectrum. The percent values mean the contribution rate of spectral intensities to represent the observed VUV spectrum.

Fig. 3. (Color online) Calculated VUV spectrum of SiH_4, using the deformed structures shown in Fig.2. The dashed line shows the supposed transition probability to the triplet excited states. The higher energy levels than 10.5 eV were not calculated here. The solid line shows the sum of the calculated VUV spectral intensities along the deformed structures depicted in Fig. 2.

Fig. 4. (Color online) The calculated potential surfaces for the excited states along (a) C_{2v} wagging mode, (b) C_{2v} stretching mode, (c) C_{3v} stretching mode of SiH_4, and (d) D_{3h} to C_{2v} wagging mode of SiH_3 radical.

Fig. 5. Reaction potentials of (a) SiH_4 + SiH_2 to Si_2H_6 and (b) Si_2H_6 + SiH_2 to Si_3H_8.

Fig. 6. Calculated reaction potentials for (a) SiH_4 + H to SiH_3 + H_2, (b) Si_2H_6 + H to Si_2H_5 + H_2, (c) Si_3H_8 + H to Si_3H_7 + H_2, and (d) Si_3H_8 + SiH_3 to Si_3H_7 + SiH_4, using B3LYP/6-311+G'd,p).

Fig. 7. Reaction potentials for Si_9H_{14} (100) + H to Si_9H_{13}(100)+ H_2 and Si_9H_{14}(100) + SiH_3 to Si_9H_{13}(100) + SiH_4, calculated using B3LYP/6-311+G(d,p).

Fig. 8. (Color online) Potential surfaces for negative and positive ions of SiH_4 as a function of Si-H bond distance, along SiH_4^+ (C_{3v}) to SiH_3^+(D_{3h}) + H and SiH_4^+ (C_s) to SiH_2^+(C_{2v}) + H_2 deformation, obtained using EOMCCSD/aug-cc-pVDZ.